Hindawi
Advances in Materials Science and Engineering
Volume 2020, Article ID 8104242, 8 pages
https://doi.org/10.1155/2020/8104242

Research Article

Effects of Anodization-Assisted Electrodeposition Conditions on the Fabrication of CuO-Cu_2O Coatings on Nanoporous Stainless Steel

Hefeng Wang,[1,2] **Jiaojiao Zhang**,[1] **and Xiaomin Jin**[1]

[1]*College of Mechanical and Vehicle Engineering, Taiyuan University of Technology, Taiyuan 030024, China*
[2]*Institute of Applied Mechanics, Taiyuan University of Technology, Taiyuan 030024, China*

Correspondence should be addressed to Hefeng Wang; wanghefeng@tyut.edu.cn

Received 4 February 2020; Revised 24 May 2020; Accepted 23 June 2020; Published 27 July 2020

Academic Editor: Fernando Lusquiños

Surface functionalization can be utilized as a useful tool to improve the antibacterial performances of medical devices. Furthermore, some antibacterial agents are coated or impregnated on the surface of 316LSS to prevent contamination of bacteria. Here, CuO-Cu_2O coatings were prepared on 316L nanoporous stainless steel (NPSS) by anodization-assisted electrodeposition for applications in antibacterial materials. The present study investigated influences of $HClO_4$ concentration, reaction temperature, and load voltage on the morphology, structure, and composition of the coatings. SEM images showed that appropriate nanopores with an average size of about 93 nm were formed on the stainless steel surface and then were successfully filled with CuO-Cu_2O. The nanopore size increased with increasing application of electrolyte concentration. Both the diameter and depth of the nanopores increased with increasing voltage. The EDX result indicated that Cu and O were embedded in as-prepared CuO-Cu_2O/NPSS. XRD analysis showed that the CuO-Cu_2O/NPSS surface comprised CuO and Cu_2O.

1. Introduction

Stainless steel (SS) with low-cost, high mechanical strength and corrosion resistance, biocompatibility, good electrical conductivity, and commercial availability has attracted much attention due to its potential applications in industrial and biomedical materials [1, 2]. However, its surface properties that allow living microorganisms to exist on SS products do not meet the health criteria. Thus, the antibacterial properties of SS must be improved.

Recently, several researchers have investigated the modification of the SS surface with nanostructures and incorporated catalysts, such as oxide metals and noble metals, to improve its catalytic properties [3–5]. For example, Rezaei et al. described the use of nanoporous SS (NPSS) containing a porous Pd film as a novel electrocatalyst/electrode design for glycerol oxidation [6]. Zhan et al. demonstrated the formation of nanopore arrays on the SS surface by anodization for visible-light photocatalytic degradation of organic pollutants [7]. Metal-based nanoporous materials with large specific surface areas, high porosity, and versatile porous structure can significantly improve utilization of surface active sites and promote chemical reactions, such as potential applications in catalysis [8–10].

Accordingly, tremendous interest has been focused on the design and fabrication of antibacterial agents (e.g., silver, copper, and zinc) on surfaces of NPSS to prevent initial adhesion of bacteria. Among these agents, copper and its oxides received intense attention due to many advantages, such as stability, cost-effectiveness, and rapid and effective bacterial killing property [11–13]. Such advantages of Cu-containing NPSS can be used in biomedical devices, such as prosthetic joints and dental implants.

Anodization has shown its excellent capability in fabricating the highly ordered nanopore structure on the surface of the metal [14, 15]. The formation of the self-organized nanoporous anodic layer onto the stainless steel

using anodization has been investigated in the literature [16–18]. From these literatures, we found that the nanostructured surface was consistent with a mixture of Cr and Fe oxides enriched in Cr_2O_3. Rezaei et al. decorated nanostructured gold within NPSS using anodic oxidation and galvanic replacement reaction, exhibiting excellent repeatability and reproducibility, long-term stability, and acceptable selectivity [14]. Wang et al. examined the use of self-organized Cu-containing nanotubes and nanopores on $Ti_{90-x}Cu_{10}Al_x$ ($x = 0$, 45) alloys, created by anodic oxidation of $Ti_{90-x}Cu_{10}Al_x$ in NH_4F-containing ethylene glycol electrolytes for the evaluation of their antimicrobial activity and cytotoxicity [15]. Simultaneously, incorporation of appropriate elements or metal oxides into well-ordered nanostructures can enhance antimicrobial activity or other electrochemical properties. Electrochemical deposition has been proved as a controllable and efficient method to fill the nanopores with metals atoms. For example, Wu et al. showed that Au nanowire arrays were successfully deposited onto the anodized aluminum oxide template by a simple and efficient combined alternate current-direct current (AC-DC) electrodeposition [19]. Ali and Maqbool showed that cobalt-nickel binary nanowires could be grown on nanoporous alumina membranes via AC electrodeposition [20]. Electrodeposition of CuO-Cu_2O on NPSS (CuO-Cu_2O/NPSS) will create a strong antibacterial material.

In this study, CuO-Cu_2O coatings were prepared on 316L nanoporous stainless steel (NPSS) by anodization-assisted electrodeposition. Then, CuO-Cu_2O/NPSS was characterized using scanning electron microscopy (SEM), X-ray diffraction (XRD), and energy-dispersive X-ray spectroscopy (EDX). The present study also investigated the influences of $HClO_4$ concentration, reaction temperature, and load voltage on the morphology of nanoporous structures.

2. Experiments

2.1. Reagents. Perchloric acid (70% $HClO_4$), ethylene glycol, $Cu(CH_3COO)_2{\cdot}H_2O$, and CH_3COONa were purchased from Tianjin Tianli Chemical Reagent Co., Ltd. Double-distilled water was used throughout the experiments.

2.2. Anodization-Electrodeposition Treatment. Prior to anodization, AISI316L SS samples ($\Phi 20\,mm \times 5\,mm$) were mounted on the resin to obtain an electrode with a square area of 1 cm^2. SS electrode samples were grounded with No. 80–1500 emery papers, followed by suspensions of diamond paste until a mirror finish was obtained, and then ultrasonically cleaned in acetone and ethanol. Electrochemical anodization was carried out in a two-electrode setup, where SS acts as the working electrode and the platinum gauze as the counter electrode. The ethylene glycol electrolyte containing different concentrations of $HClO_4$ was used as the electrolyte. A DC voltage stabilizer provided a constant potential between working and counter electrodes with the anodizing duration of different anodizing time. During anodization, the electrolyte was vigorously stirred or not stirred, and its temperature was maintained at 0°C. The anodized electrode was then ultrasonically washed in ethanol and distilled water for 10 min and dried in a nitrogen stream.

Table 1: Electrodeposition experiment parameters of CuO-Cu_2O/NPSS.

Number	Temperature	Electrolyte concentration
A	20	0.02 M $Cu(CH_3COO)_2 \cdot H_2O$ + 0.1 M CH_3COONa
B	20	0.1M $Cu(CH_3COO)_2 \cdot H_2O$ + 0.1 M CH_3COONa
C	60	0.02 M $Cu(CH_3COO)_2 \cdot H_2O$ + 0.1 M CH_3COONa
D	60	0.1M $Cu(CH_3COO)_2 \cdot H_2O$ + 0.1 M CH_3COONa

Electrodeposition was carried out using the Gamry Reference 600 electrochemical workstation, with the NPSS sample acting as a working electrode, a saturated calomel electrode (SCE) as the reference electrode, and the platinum mesh electrode as a counter electrode. CuO-Cu_2O coatings were electrodeposited onto the surface of NPSS at a cathode potential of −1.0 V versus SCE for 3600 s. Influences of electrolyte concentration and deposition temperature on the morphology of CuO-Cu_2O/NPSS were investigated. Table 1 lists the specific process numbers, electrolyte concentrations, and deposition temperature parameters. Figure 1 displays the preparation procedure of CuO-Cu_2O/NPSS. CuO-Cu_2O coatings were prepared on 316L nanoporous stainless steel (NPSS) by anodization-assisted electrodeposition.

2.3. Microstructural Characterization. Phases of NPSS and CuO-Cu_2O/NPSS were identified by Rigaku DyMax2500 XRD with the 1.5410 Å Cu *Kα* line as an excitation source. Morphology, structure, and compositional distribution of NPSS and CuO-Cu_2O/NPSS were characterized by a field-emission scanning electron microscope (JSM-7001F, JEOL), equipped with the energy-dispersive X-ray (QX-200, Bruker).

3. Results and Discussion

3.1. Anodization

3.1.1. Effect of Electrolyte Concentration. Influences of three processing factors, namely, $HClO_4$ concentration, temperature, and load voltage, on nanopores were investigated.

Figure 2 shows the microstructure of the nanoporous surface prepared in a $HClO_4$ solution with different concentrations on SS under 50 V voltage at 0°C for 600 s. As shown in Figure 2, the pore size of nanopores formed by a 3 vol% electrolyte $HClO_4$ solution is smaller than that of the 5 vol% electrolyte $HClO_4$ solution, and nanopores exhibited characteristics of strip distribution [21, 22]. The nanoporous surface prepared in the electrolyte $HClO_4$ solution at 5 vol% concentrations was distributed homogeneously and exhibited appropriate pore size. However, the

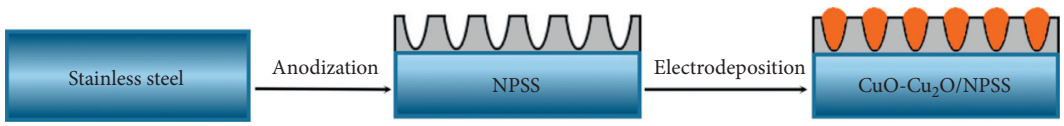

Figure 1: Schematic illustration of the procedure for preparing CuO-Cu_2O/NPSS.

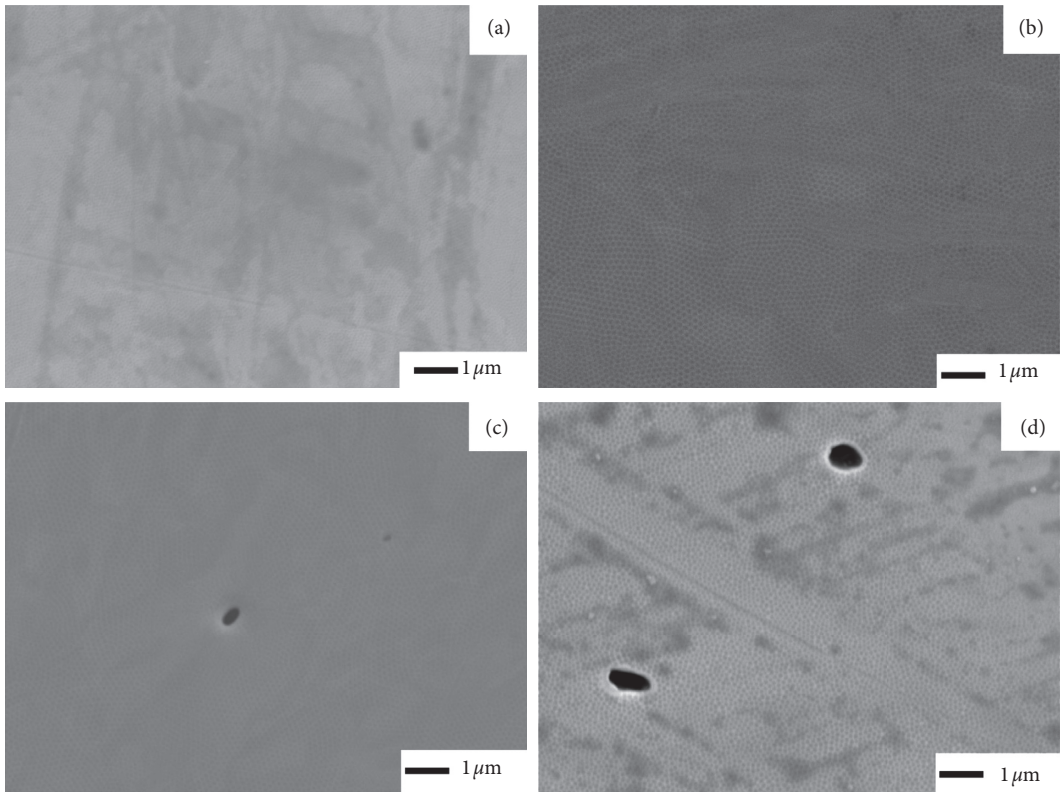

Figure 2: SEM images of stainless steel samples anodized under different $HClO_4$ solution concentrations: (a) 3 vol%, (b) 5 vol%, (c) 7 vol%, and (d) 9 vol%.

microstructure of the nanoporous surface prepared in an electrolyte $HClO_4$ solution at 7 and 9 vol% concentrations exhibited different degrees of pitting corrosion [23], and nanopore walls became thinner. Overall, the nanopore size increased with increasing application of electrolyte concentration, which is in line with expected outcomes and literature [24]. In the following experiments, the 5 vol% electrolyte $HClO_4$ solution was used as the electrolyte.

3.1.2. Effect of Load Voltage. Figure 3 illustrates the microstructures of the 316L stainless steel at different anodizing voltages. The nanopore structure can be formed on the surface of the 316L stainless steel (Figure 3). The load voltage is one of the most important influential factors in the formation of the nanoporous structure. Both the diameter and depth of the nanopores increase with increasing voltage. An ideal nanopores structure can be obtained at voltages of 40 and 50 V (see Figures 3(c) and 3(d)). It was found that the nanopore structure obtained at 50 V is slightly larger than that at 40 V, with estimated values of 93 and 87 nm, respectively. In the following experiments, SS samples were anodized at 50 V.

3.1.3. Effect of Anodizing Time. Figure 4 illustrates the microstructures of the 316L stainless steel in a 5 vol% electrolyte $HClO_4$ solution at different times under 50 V voltage. Corrosion accelerated with increasing anodizing time. The color of the electrolyte turned rapidly from colorless to tan. Figure 4(a) indicates the nanopore structure prepared at 300 s. The homogeneous porous structure and some large pores were formed at an anodization time of 600 s (as shown in Figure 4(b)). Thin nanopore walls were detected, and irregular nanopore sizes were anodized at 1800 s. The microstructure of the nanoporous surface prepared at an anodization time of 3600 s showed different degrees of pitting. In the following experiments, the anodization time of 600 s was used as the anodizing time.

Anodic oxidation current was recorded each second during anodization at 3600 s. Figure 5 shows the resulting current against time plots. A sharp falling and rising of the current were noted at short anodization times ($t < 120$ s). The

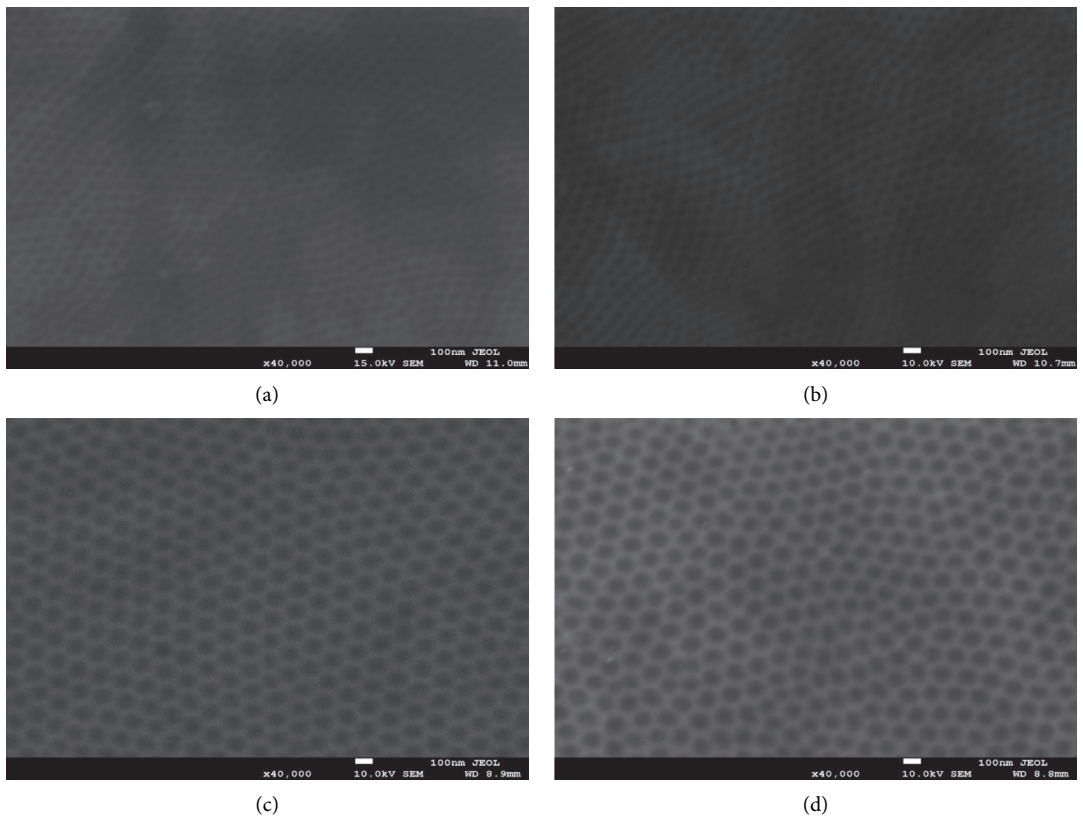

Figure 3: SEM images of stainless steel samples anodized under different load voltages: (a) 20 V, (b) 30 V, (c) 40 V, and (d) 50 V.

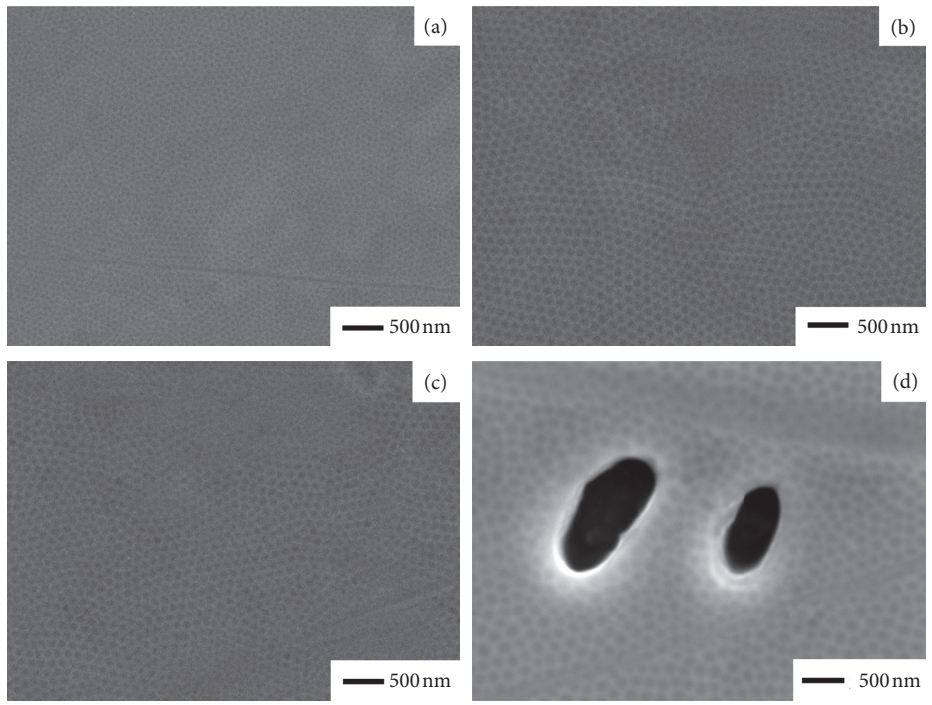

Figure 4: SEM images of stainless steel samples anodized under different anodizing times: (a) 300 s, (b) 600 s, (c) 1800 s, and (d) 3600 s.

decline in the current may be ascribed to nucleation and growth of pores on the barrier layer. These observations support the conclusions derived from current against time responses recorded during anodization (Figure 4(b)) and indicate that anodizing at 600 s provides the best nanopore size.

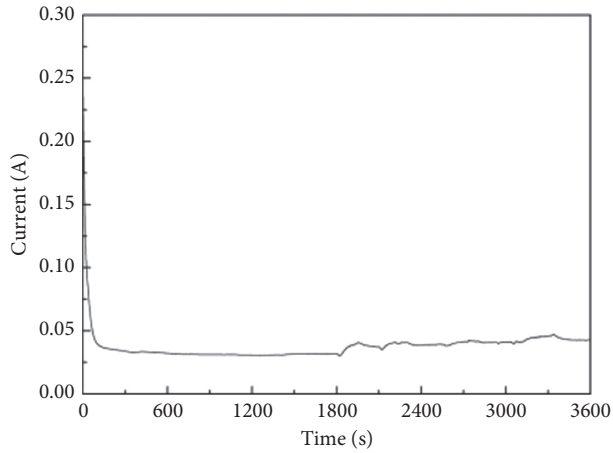

Figure 5: The *I-t* curve of stainless steel samples anodized.

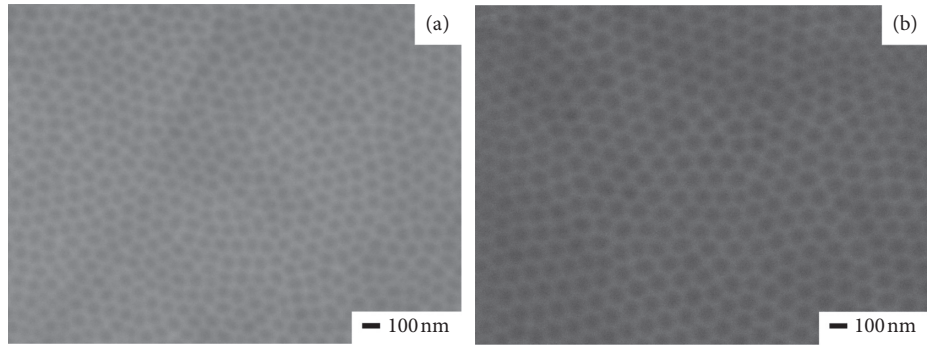

Figure 6: SEM images of stainless steel samples anodized under different stirring: (a) without stirring and (b) with stirring.

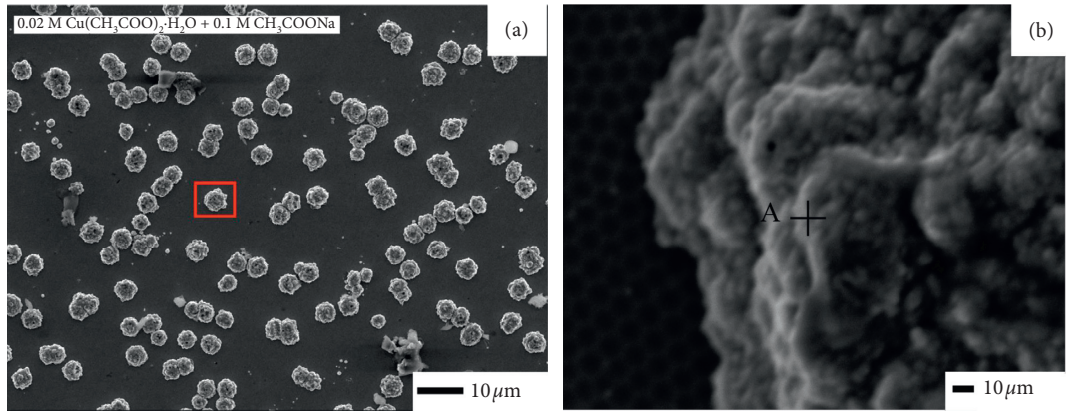

Figure 7: SEM images of electrodeposition of the CuO-Cu_2O film on NPSS under A.

3.1.4. Effect of Stirring. Figure 6 compares the results of anodic oxidation of SS with or without magnetic stirring. SEM images show relatively uniform pore size obtained by anodic oxidation with uniform magnetic stirring and larger pore size.

An appropriate nanoporous structure with a mean diameter of 93 nm was obtained on the SS surface by the following conditions: 5 vol% electrolyte $HClO_4$ solution; 50 V load voltage; 600 s reaction time; reaction with uniform magnetic stirring.

3.2. Electrodeposition. Copper is easily electrodeposited at a low overpotential. In the present work, Cu was

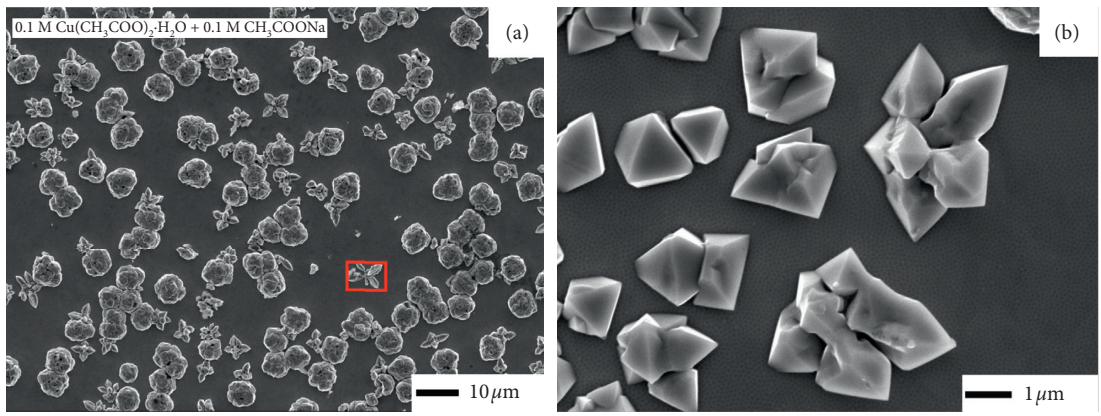

Figure 8: SEM images of electrodeposition of the CuO-Cu_2O film on NPSS under B.

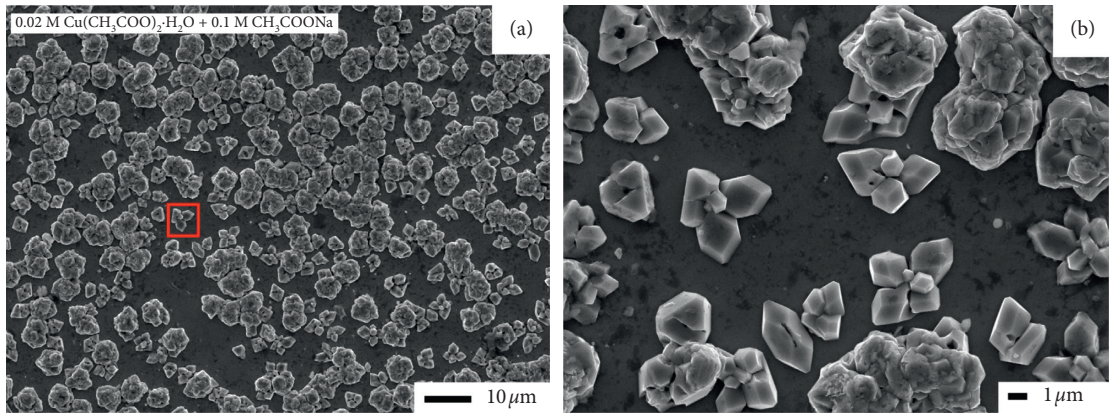

Figure 9: SEM images of electrodeposition of the CuO-Cu_2O film on NPSS under C.

electrodeposited onto nanopores of the NPSS electrode at a cathode potential of −1.0 V versus SCE for 3600 s.

Figure 7(a) shows that numerous flower-like deposits were formed on the surface of NPSS under conditions of process A. As indicated in Figure 7(b), nanopores on the SS surface were observed, and the deposited CuO-Cu_2O formed by electrochemical deposition incompletely covered the surface.

In addition to the formation of more uniformly distributed branched copper oxide, flower-like copper deposits were formed on the SS surface (as shown in Figure 8(a)). As displayed in Figure 8(b), the remaining nanopores were detected around copper deposits formed by electrodeposition, and the prepared porous CuO-Cu_2O film does not cover the surface. Considering the effect of temperature, nanopores were still present around copper deposits formed by electrodeposition at 20°C. In the following experiments, 60°C was used as the deposition temperature.

As shown in Figure 9, the surface of SS nanopores is densely distributed with deposited CuO-Cu_2O, and a regular cubic crystal structure of CuO exists on the NPSS surface.

Figures 10(a) and 10(b) show the morphological changes of the CuO-Cu_2O/NPSS surface with different magnifications. CuO-Cu_2O coatings have been successfully grown on the surface of NPSS. Analysis of coating morphologies revealed the copper dendritic crystals formed by electrodeposition. These coating morphologies agree with those recently reported [25]. Formation of dendritic deposits is a primary characteristic of electrodeposition at overpotentials belonging to the plateau of limiting diffusion current density, whereas induction time of dendritic growth initiation depends on the overpotential of electrodeposition [26, 27]. The mechanism of typical copper dendritic structures is explained based on the diffusion-limited aggregation (DLA) model [25] because polycrystalline copper branches are a typical characteristic of DLA-like copper deposits. This result indicates that NPSS-assisted electrodeposition is an important technique for synthesizing metallic nanomaterials with controlled shape and size. Such a porous layer has a high surface area and excellent antibacterial properties. Figure 10(b) illustrates the EDX results of CuO-Cu_2O/NPSS. Combined with XRD results, electrodeposition has formed copper oxide.

Appropriate CuO-Cu_2O/NPSS was obtained by the following conditions: 0.1 M $Cu(CH_3COO)_2{\cdot}H_2O$ + 0.1 M CH_3COONa solution and 60°C deposition temperature.

3.3. XRD Analyses of CuO-Cu_2O/NPSS Samples. Figure 11 shows the XRD spectra of CuO-Cu_2O/NPSS. In Figure 11, the presence of Cu_2O and CuO diffraction peaks

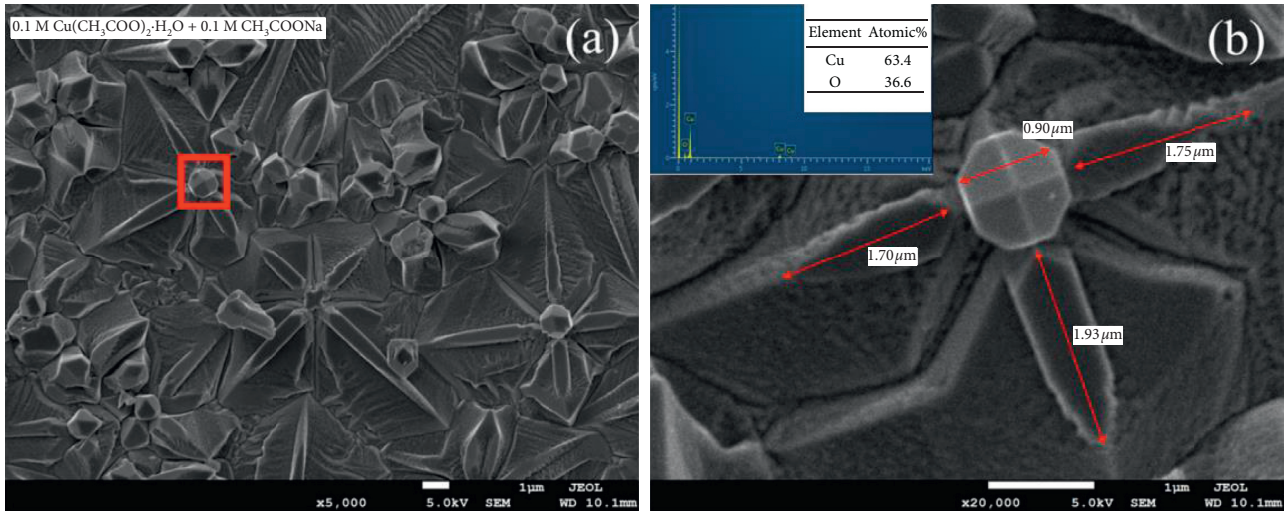

Figure 10: SEM images of electrodeposition of the CuO-Cu_2O film on NPSS under D. The inset shows the corresponding elemental atomic ratios.

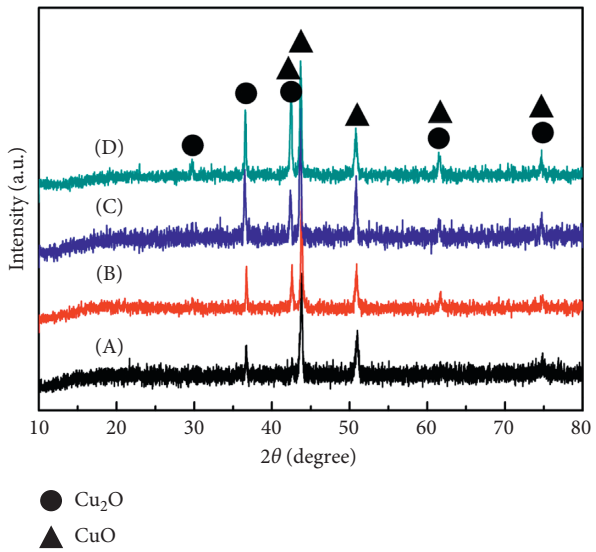

Figure 11: XRD spectra of CuO-Cu_2O/NPSS.

can be seen. The appearance of the Cu_2O phase agrees with a previous report [24]. Zhu et al. reported that the nanoporous surface of the Ti-Cu amorphous alloy consists of TiO, Ti_2O_3, TiO_2, and Cu_2O [24]. The presence of Cu_2O and CuO phases was reasonable for the bactericidal effect.

4. Conclusions

In summary, a porous CuO-Cu_2O film on NPSS was successfully fabricated by anodization-assisted electrodeposition. The present study investigated influences of $HClO_4$ concentration, reaction temperature, and load voltage on the morphology of the nanoporous structure. An appropriate nanoporous structure with a mean diameter of 93 nm was obtained on the SS surface by the following conditions: 5 vol % electrolyte $HClO_4$ solution; 50 V load voltage; 600 s reaction time; reaction with uniform magnetic stirring. Appropriate CuO-Cu_2O/NPSS was obtained by the following conditions: 0.1 M $Cu(CH_3COO)_2·H_2O$ + 0.1 M CH_3COONa solution and 60°C deposition temperature. XRD analysis shows that the CuO-Cu_2O/NPSS surface comprises CuO and Cu_2O.

Data Availability

Any reader or researcher who wishes to obtain the research data of this article can contact the author by e-mail.

Conflicts of Interest

The authors declare no conflicts of interest.

Acknowledgments

The authors would like to thank the financial support from the National Natural Science Foundation of China (51171125 and 11172195), National Science Foundation for Distinguished Young Scholars of China (E010101), Shanxi Province Programs for Science and Technology Development (20110321051), Post-Doctoral Science Fund of China (2013M541209), Youth Foundation of Taiyuan University of Technology (2012L073), Natural Science Foundation for Young Scientists of Shanxi Province (2013021013-5), and Shanxi Province Nature Science Fund (2012011021-3).

References

[1] A. Bekmurzayeva, W. J. Duncanson, H. S. Azevedo, and D. Kanayeva, "Surface modification of stainless steel for biomedical applications: revisiting a century-old material," *Materials Science and Engineering: C*, vol. 93, pp. 1073–1089, 2018.

[2] J. Zhao, Z. Zhai, D. Sun et al., "Antibacterial durability and biocompatibility of antibacterial-passivated 316L stainless steel in simulated physiological environment," *Materials Science and Engineering: C*, vol. 100, pp. 396–410, 2019.

[3] Z. Liu, B. Liu, D. Ding, Z. Jiang, and C. Xia, "Development of three-layer intermediate temperature solid oxide fuel cells with direct stainless steel based anodes," *International Journal of Hydrogen Energy*, vol. 37, no. 5, pp. 4401–4405, 2012.

[4] M. Yao, B. Sun, N. Wang, W. Hu, and S. Komarneni, "Self-generated N-doped anodized stainless steel mesh for an efficient and stable overall water splitting electrocatalyst," *Applied Surface Science*, vol. 480, pp. 655–664, 2019.

[5] L. Sheng, G. Li, W. Zhang, and K. Wang, "Full-stainless steel mesh dye-sensitized solar cells based on core-shell ZnO/TiO_2 nanorods," *Optik*, vol. 184, pp. 90–97, 2019.

[6] B. Rezaei, E. Havakeshian, and A. A. Ensafi, "Fabrication of a porous Pd film on nanoporous stainless steel using galvanic replacement as a novel electrocatalyst/electrode design for glycerol oxidation," *Electrochimica Acta*, vol. 136, pp. 89–96, 2014.

[7] W. Zhan, H. Ni, R. Chen, X. Song, K. Huo, and J. Fu, "Formation of nanopore arrays on stainless steel surface by anodization for visible-light photocatalytic degradation of organic pollutants," *Journal of Materials Research*, vol. 27, no. 18, pp. 2417–2424, 2012.

[8] P. Roy, S. Berger, and P. Schmuki, "TiO_2 nanotubes: synthesis and applications," *Angewandte Chemie International Edition*, vol. 50, no. 13, pp. 2904–2939, 2011.

[9] Y.-C. Nah, I. Paramasivam, and P. Schmuki, "Doped TiO_2 and TiO_2 nanotubes: synthesis and applications," *ChemPhysChem*, vol. 11, no. 13, pp. 2698–2713, 2010.

[10] Y. Q. Liang, Z. D. Cui, S. L. Zhu, Y. Liu, and X. J. Yang, "Silver nanoparticles supported on TiO_2 nanotubes as active catalysts for ethanol oxidation," *Journal of Catalysis*, vol. 278, no. 2, pp. 276–287, 2011.

[11] K. Kumar, A. Priya, A. Arun, S. Hait, and A. Chowdhury, "Antibacterial and natural room-light driven photocatalytic activities of CuO nanorods," *Materials Chemistry and Physics*, vol. 226, pp. 106–112, 2019.

[12] O. Akhavan and E. Ghaderi, "Cu and CuO nanoparticles immobilized by silica thin films as antibacterial materials and photocatalysts," *Surface and Coatings Technology*, vol. 205, no. 1, pp. 219–223, 2010.

[13] S. Usefi, K. Akhbari, and J. White, "Sonochemical synthesis, structural characterizations and antibacterial activities of biocompatible Copper(II) coordination polymer nanostructures," *Journal of Solid State Chemistry*, vol. 276, pp. 61–67, 2019.

[14] B. Rezaei, E. Havakeshian, and A. A. Ensafi, "Decoration of nanoporous stainless steel with nanostructured gold via galvanic replacement reaction and its application for electrochemical determination of dopamine," *Sensors and Actuators B: Chemical*, vol. 213, pp. 484–492, 2015.

[15] X. Wang, J. Qiao, F. Yuan, R. Hang, X. Huang, and B. Tang, "In situ growth of self-organized Cu-containing nano-tubes and nano-pores on $Ti_{90-x}Cu_{10}Al_x$ ($x = 0, 45$) alloys by one-pot anodization and evaluation of their antimicrobial activity and cytotoxicity," *Surface and Coatings Technology*, vol. 240, pp. 167–178, 2014.

[16] F. Martin, D. Del Frari, J. Cousty, and C. Bataillon, "Self-organisation of nanoscaled pores in anodic oxide overlayer on stainless steels," *Electrochimica Acta*, vol. 54, no. 11, pp. 3086–3091, 2009.

[17] K. Kure, Y. Konno, E. Tsuji, P. Skeldon, G. E. Thompson, and H. Habazaki, "Formation of self-organized nanoporous anodic films on Type 304 stainless steel," *Electrochemistry Communications*, vol. 21, pp. 1–4, 2012.

[18] H. Tsuchiya, T. Suzumura, Y. Terada, and S. Fujimoto, "Formation of self-organized pores on type 316 stainless steel in organic solvents," *Electrochimica Acta*, vol. 82, pp. 333–338, 2012.

[19] Z. Wu, Y. Zhang, and K. Du, "A simple and efficient combined AC-DC electrodeposition method for fabrication of highly ordered Au nanowires in AAO template," *Applied Surface Science*, vol. 265, pp. 149–156, 2013.

[20] G. Ali and M. Maqbool, "Fabrication of cobalt-nickel binary nanowires in a highly ordered alumina template via AC electrodeposition," *Nanoscale Research Letters*, vol. 8, pp. 1–8, 2013.

[21] Y. Xu, A. S. Menon, P. P. R. M. L. Harks et al., "Honeycomb-like porous 3D nickel electrodeposition for stable Li and Na metal anodes," *Energy Storage Materials*, vol. 12, pp. 69–78, 2018.

[22] V. Vignal, J. C. Roux, S. Flandrois, and A. Fevrier, "Nanoscopic studies of stainless steel electropolishing," *Corrosion Science*, vol. 42, no. 6, pp. 1041–1053, 2000.

[23] E. Salahinejad, R. Eslami Farsani, and L. Tayebi, "Synergistic galvanic-pitting corrosion of copper electrical pads treated with electroless nickel-phosphorus/immersion gold surface finish," *Engineering Failure Analysis*, vol. 77, pp. 138–145, 2017.

[24] S. L. Zhu, J. L. He, X. J. Yang, Z. D. Cui, and L. L. Pi, "Ti oxide nano-porous surface structure prepared by dealloying of Ti-Cu amorphous alloy," *Electrochemistry Communications*, vol. 13, no. 3, pp. 250–253, 2011.

[25] N. D. Nikolić, K. I. Popov, L. J. Pavlović, and M. G. Pavlović, "Morphologies of copper deposits obtained by the electrodeposition at high overpotentials," *Surface and Coatings Technology*, vol. 201, no. 3-4, pp. 560–566, 2006.

[26] K. Popov, N. Nikolic, and Z. Rakocevic, "An estimation of the interfacial energy of the copper-copper sulphate solution interface and of the specific surface of copper powder," *Journal of the Serbian Chemical Society*, vol. 67, no. 8-9, pp. 635–638, 2002.

[27] K. Popov, N. Nikolic, and Z. Rakocevic, "The estimation of solid copper surface tension in copper sulfate solutions," *Journal of the Serbian Chemical Society*, vol. 67, no. 11, pp. 769–775, 2002.